

In silico optimization of phase-change materials for digital memories: a survey of first-row transition-metal dopants for $\text{Ge}_2\text{Sb}_2\text{Te}_5$

This content has been downloaded from IOPscience. Please scroll down to see the full text.

View [the table of contents for this issue](#), or go to the [journal homepage](#) for more

Download details:

IP Address: 149.132.2.57

This content was downloaded on 29/05/2016 at 16:24

Please note that [terms and conditions apply](#).

In silico optimization of phase-change materials for digital memories: a survey of first-row transition-metal dopants for $\text{Ge}_2\text{Sb}_2\text{Te}_5$

J M Skelton and S R Elliott

Department of Chemistry, University of Cambridge, Cambridge CB2 1EW, UK

E-mail: sre1@cam.ac.uk


Received 18 March 2013, in final form 14 April 2013

Published 30 April 2013

Online at stacks.iop.org/JPhysCM/25/205801

Abstract

Phase-change materials are the alloys at the heart of an emerging class of next-generation, non-volatile digital memory technologies. However, the widely studied Ge–Sb–Te system possesses several undesirable properties, and enhancing its properties, e.g. by doping, is an area of active research. Various first-row transition-metal dopants have been shown to impart useful property enhancements, but a systematic study of the entire period has yet to be undertaken, and little has been done to investigate their interaction with the host material at the atomic level. We have carried out first-principles computer simulations of the complete phase-change cycle in $\text{Ge}_2\text{Sb}_2\text{Te}_5$ doped with each of the ten first-row transition metals. In this article, we present a comprehensive survey of the electronic, magnetic and optical properties of these doped materials. We discuss in detail their atomic-level structure, and relate the microscopic behaviours of the dopant atoms to their influence on the $\text{Ge}_2\text{Sb}_2\text{Te}_5$ host. By considering an entire family of similar materials, we identify trends and patterns which might be used to predict suitable dopants for optimizing materials for specific phase-change applications. The computational method employed here is general, and this materials-discovery approach could be applied in the future to study other families of potential dopants for such materials.

 Online supplementary data available from stacks.iop.org/JPhysCM/25/205801/mmedia

(Some figures may appear in colour only in the online journal)

1. Introduction

Phase-change random-access memory (PCRAM) is one of the leading contenders for an upcoming generation of post-Si electronic memories [1]. Its operation is based on the reversible switching of a phase-change material (PCM) between amorphous and crystalline phases with measurably different electrical properties [2], which allows binary information to be encoded in the material structure. PCRAM devices have the potential for ultrafast [3], even sub-nanosecond [4], switching speeds, low power consumption [5, 6], high write endurance [6], and excellent size scaling [5, 7].

Furthermore, the data density may be improved beyond the scaling limit by multilevel programming, thereby storing more than one bit per cell [8]. Together with inherently non-volatile operation, these qualities could allow PCRAM to function as a ‘universal memory’ [9], combining the best characteristics of both flash memory and DRAM [10].

Two PCMs, namely GeTe– Sb_2Te_3 (GST) pseudobinary alloys [11] and Ag/In-doped Sb_2Te_3 (AIST) [12], are used in commercially-available rewritable optical discs, in which reflectance contrasts between the amorphous and crystalline phases are exploited to store data. The former system has become the prototypical PCM for PCRAM

research, and has been widely studied in electrically-switched memories. Despite this success, however, GST possesses several undesirable properties. These include a relatively low crystallization temperature and activation energy, limiting its data-retention capability, and a high melting temperature, which necessitates a high electrical power for amorphization [1, 10]. Amorphous GST also suffers from ‘resistance drift’, where the resistance of the material displays a power-law increase with time [13]. This is a particular problem for multilevel storage, since it limits the number of resistance levels that can be reliably held in a single cell [13], and increases the complexity of readout codes [13, 14].

In light of these issues, a number of alternative PC material systems have been investigated, including GeTe [15], various Ga–Sb–Te [16] alloys, and a range of binary antimonides [17–19]. Investigating novel systems can involve significant trial and error, however, not least because of the contradictory need for good amorphous-phase stability and fast crystallization speeds. Enhancing the properties of GST by doping has thus been another widely pursued avenue of research. P-block elements, including C [20], N [21], O [22] and Si [23], have been commonly employed for this purpose. A range of transition-metal (TM) dopants have also been investigated, including Mn [24], Fe [25, 26], Zn [26] and Mo [27]. Interestingly, it has been shown that, with Fe, a magnetic, as well as electrical, contrast between phases could be achieved, offering an additional readout method and giving such doped materials a potential application in so-called spin-electronic (‘spintronic’) devices [28].

To enable a more rational approach to designing PCMs, it is important to understand the physics underpinning their properties and behaviour. First-principles computer simulations have proved to be a valuable complement to experiment in this regard, giving atomic-level insight into the structure and unusual properties of PCMs [29–32]. *Ab initio* molecular-dynamics (AIMD) simulations have been used to understand the origin of the fast phase transition [33, 34], together with related issues such as the role of the intrinsic vacancies in GST materials [35], and the effect of pre-annealing on crystallization dynamics [4]. First-principles calculations have also been used to investigate doped GST, including with p-block dopants [36, 37] and the transition metals Fe [38], Mn and Zn [39], and Cr, Mn, Co and Ni [40].

However, a systematic study of the entire first-row of TMs has not previously been undertaken. With a family of notionally quite similar dopants, such a study might reveal trends and patterns in their influence on the properties of GST hosts, which could be used predictively to select suitable TM dopants for specific applications. In this work, we have carried out a comprehensive AIMD survey of $\text{Ge}_2\text{Sb}_2\text{Te}_5$ doped with each of the ten first-row TMs. We focus in particular on the technologically-relevant electrical, optical and magnetic properties of the doped materials, and relate these to their atomic structure. Our results reveal several interesting trends which not only give valuable insight into the interaction of TM dopants with a $\text{Ge}_2\text{Sb}_2\text{Te}_5$ host, but, importantly, show what sort of effects they might have on its physical properties.

2. First-principles simulations

Molecular-dynamics simulations of the melt-quench-anneal phase-change cycle were carried out using the VASP code [41]. Each doped model was created in a cubic supercell containing 99 host atoms and one TM atom, giving an ~ 1 at.% dopant concentration. This represents a dilute case, but allows the investigation to focus on the dopant atoms.

Random initial configurations were mixed at 3000 K for 20 ps and maintained in a liquid state at 1200 K for a further 40 ps. The temperature was then reduced to 300 K at a rate of 15 K ps^{-1} , which invariably led to amorphization. The amorphous models were annealed at 600 K for 250–500 ps to crystallize them. The final amorphous and crystalline models were energy-relaxed, with the cell shape and volume allowed to vary, and calculations of various properties, e.g. electronic densities of states, ground-state magnetization and reflectance, were carried out on these relaxed models.

Where applicable, property calculations were carried out with the TM atoms in their lowest energy magnetic state. To determine this, we took the relaxed model and recalculated the ground-state electronic wavefunctions starting with 0, 1, 2, 3, 4 and 5 unpaired electrons on the dopant atom, mimicking 0–5 unpaired d electrons. After wavefunction minimization, we noted the magnetization and total energy of the models, relative to the non-magnetic state found by setting an initial magnetic moment of zero, and took the magnetic ground-state to be that with the lowest energy.

During the MD runs, the densities of the systems were fixed at 6.11 g cm^{-3} , intermediate between the experimental amorphous and crystalline densities of undoped $\text{Ge}_2\text{Sb}_2\text{Te}_5$. We used a 5 fs timestep, and employed a velocity-rescaling algorithm to maintain the temperature. In order to verify the simulation results, each simulation was repeated twice, starting from different initial configurations.

The PBE exchange–correlation functional [42] was used with projector augmented-wave (PAW) pseudopotentials [43], together with the highest of the energy cutoffs recommended in the pseudopotential files¹. Cell relaxations and property calculations were run with a $1.3\times$ larger cutoff. The MD simulations and cell relaxations were carried out using the gamma point to sample the Brillouin zone, while the property calculations were done using a denser $2\times 2\times 2$ gamma-centred Monkhorst–Pack grid [44]. Accurate calculation of optical properties requires a large number of conduction bands, and thus the number of bands was increased to 1200 (roughly triple the default) for the reflectance simulations. For consistency, and because we were unsure *a priori* which of the doped systems might contain unpaired electrons, we opted to use spin polarization in all simulations.

3. Electronic structure and magnetic properties

The influence of a dopant on the electronic structure of the host is an important consideration, since various key

¹ See electronic supplementary material, available online at stacks.iop.org/JPhysCM/25/205801/mmedia.

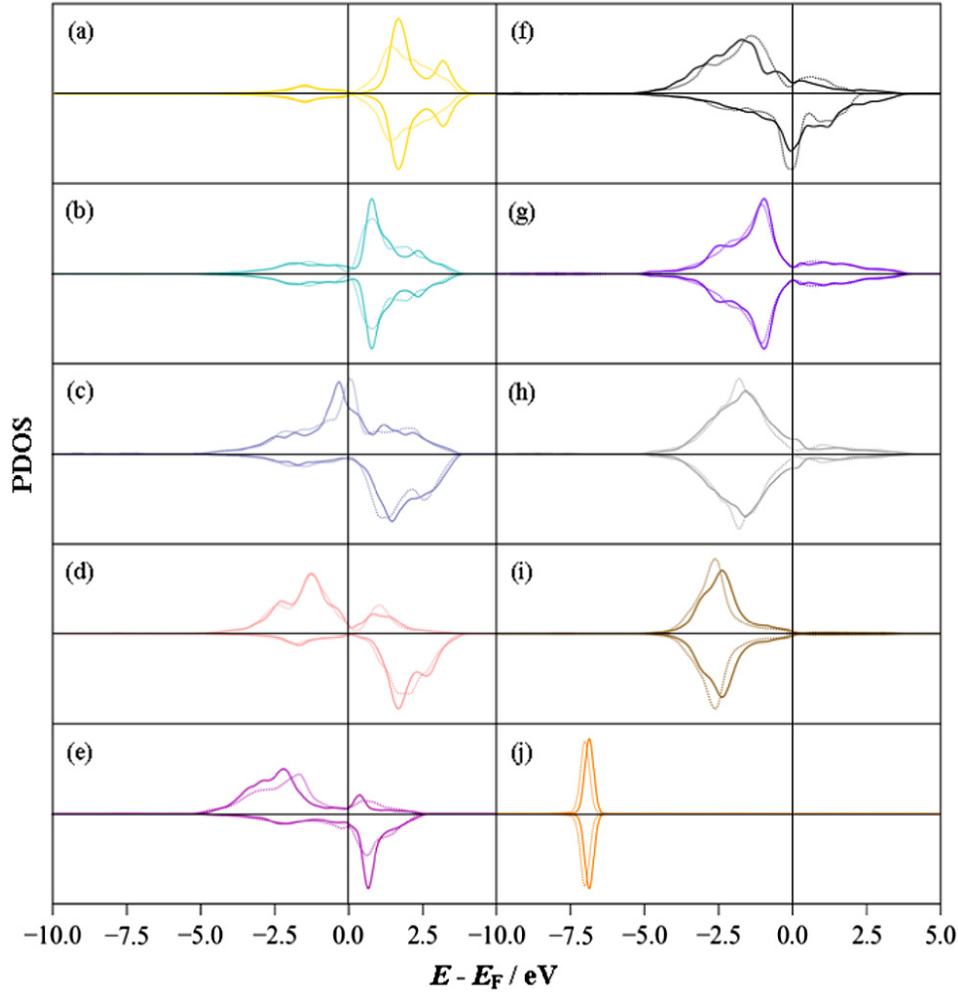


Figure 1. Simulated partial density of states (PDOS) curves for transition-metal (TM)-doped $\text{Ge}_2\text{Sb}_2\text{Te}_5$. The plots show the position of the TM d states with respect to the Fermi level in the amorphous (dashed line) and crystalline (solid line) phases, for Sc (a) to Zn (j). In all ten figures, the spin-up PDOS is plotted on the positive axis, and the spin-down PDOS on the negative axis. The colour coding of the lines is as follows: Sc—yellow, Ti—cyan, V—steel blue, Cr—pink, Mn—purple, Fe—black, Co—violet, Ni—silver, Cu—copper, Zn—orange.

physical properties—in particular resistivity and optical absorption—depend upon it. To investigate this, we calculated partial density of states (PDOS) curves for each of the relaxed amorphous and crystalline structures. Although the overall form of the host DOS is relatively unaffected by the presence of the dopant (see footnote 1), the TM d states are of sufficiently high energy to contribute to the valence and conduction bands (figure 1), and can therefore lead to subtle changes. We found that the Sc d states lay almost entirely within the conduction band, while the Zn states lay deep within the valence band. On traversing the period, the d states systematically move across the bandgap, and, for the elements Ti to Ni, the d states lie within both bands. The lowering in energy of the d states for elements from Sc–Zn is expected from the increase in nuclear charge across the period, and the fact that, for many TMs, the d states lie near band edges, suggests that TM dopants could be used to ‘fine-tune’ the features near the bandgap, significantly influencing electrical and optical properties.

Our DFT calculations failed to reproduce the bandgap in either of the insulating amorphous and semiconducting

crystalline phases of undoped $\text{Ge}_2\text{Sb}_2\text{Te}_5$ (see footnote 1). Although the number of states falls either side of the Fermi energy in the simulated DOS curves, it does not go to zero. We also found that, in the amorphous phase, the calculated Fermi energy was pinned near the top of the valence band, rather than occurring at the point where the DOS reached a minimum.

Although these issues could be due in part to our relatively small models, especially in the case of the amorphous phase, the Kohn–Sham [45] density-functional theory scheme used in these simulations is known typically to underestimate bandgaps [46]. In light of this, and since, in the cases where the TM d states straddle the Fermi energy, the d state DOS decreases either side of the gap, it is likely that the non-metallic nature of the host material would be preserved on doping, at least for most of the dopants.

It is also evident from the plots in figures 1(c)–(f) that the elements V to Fe have magnetic ground-states, leading to differences in the spin up/down DOS either side of the Fermi energy. To investigate magnetic properties in more detail, we compared the relative energies of electronic configurations

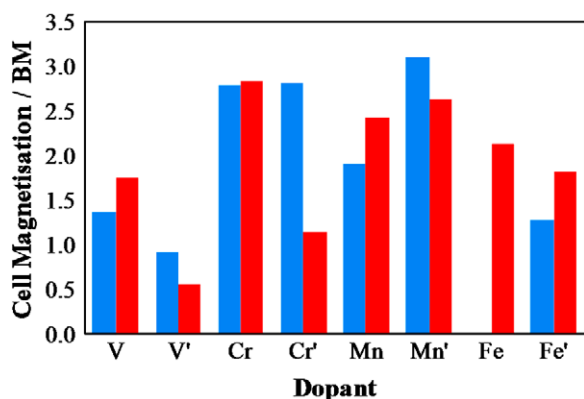


Figure 2. Magnetic properties of transition metal-doped $\text{Ge}_2\text{Sb}_2\text{Te}_5$. The figure shows the magnetization of the simulation cell for the electronic ground-states of amorphous (blue bars, left) and crystalline (red bars, right) phases of $\text{Ge}_2\text{Sb}_2\text{Te}_5$ doped with V, Cr, Mn and Fe. Results for both runs are shown side by side, with calculations from the second set of simulations denoted by a prime beside the chemical symbol.

found, starting from 0–5 unpaired electrons on the TM atoms, taking the non-magnetic state as a zero reference (see footnote 1).

We found that Sc, Ti, Co, Ni and Zn exhibited no magnetic states, while Cu generally had one magnetic state in both phases, but these invariably lay at a large energy of 1.7–4.5 eV above the (non-magnetic) ground-state. In contrast, V to Fe all exhibited one or more low-energy magnetic states. The ground-state magnetization for these atoms in the amorphous and crystalline phases, in both sets of simulations, is compared in figure 2.

Our findings are in line with those in [40], in which Cr and Mn were found to have magnetic ground-states when doped into $\text{Ge}_2\text{Sb}_2\text{Te}_5$, while Co and Ni were not magnetic. Magnetic ground-states were consistently observed for elements V to Fe in both the amorphous and crystalline models, save for one amorphous Fe-doped model, in which the electronic ground-state had zero magnetization. This discrepancy is likely to be due to the magnetic moments being sensitive to the local geometry of the dopants, as reported in [38, 40, 47], which is also reflected in the ground-state magnetism of all four atoms being different in both sets of simulations.

The results of these calculations thus suggest that the elements V to Fe may, when doped into $\text{Ge}_2\text{Sb}_2\text{Te}_5$, introduce magnetic properties. The TMs generally exhibit a difference in magnetism between the two phases, as has already been reported for Fe-doped materials [25, 38], and thus it may be possible to harness this as an additional property contrast in memory devices. However, with single dopant atoms in the models, we cannot investigate magnetic exchange, nor can we obtain detailed statistics, and further work is currently underway to study the magnetic behaviour of bulk systems. Nonetheless, these findings suggest that some TM dopants may yield materials that allow phase-change technology to be merged with spintronics [28], and they are in line with the identification of several TM-containing GeTe materials,

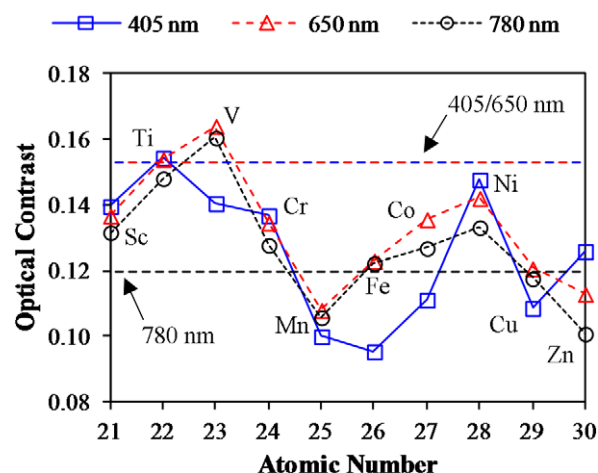


Figure 3. Optical contrast in transition-metal (TM)-doped $\text{Ge}_2\text{Sb}_2\text{Te}_5$. This plot compares the optical contrast in the doped models at three technologically-important laser wavelengths, namely 405 nm (blue, squares), 650 nm (red, triangles) and 780 nm (black, circles). Each point is the average of the values calculated from both sets of simulations (see footnote 1). The calculated optical contrast of the undoped system is overlaid as red/blue (405/650 nm) and black (780 nm) dashed lines for comparison.

including $\text{Ge}_{1-x}\text{Cr}_x\text{Te}$ [48], $\text{Ge}_{1-x}\text{Mn}_x\text{Te}$ [49] and Fe-doped GeTe [50], as magnetic semiconductors.

4. Optical properties

Although much current research focuses on electrically-switched PCM devices, it is also of interest to see how the dopants influence the optical properties of $\text{Ge}_2\text{Sb}_2\text{Te}_5$. We simulated the dielectric functions of the undoped and ten doped models, from which we calculated reflectance spectra (see footnote 1), and hence computed the optical contrast, according to the definition in [51], at the technologically-relevant wavelengths of 780 nm (compact disc), 650 nm (digital versatile disc) and 405 nm (Blu-Ray). These values are presented in figure 3, where they are compared to the corresponding values for the undoped model.

In our simulations, most of the TM dopants, save for Mn, improved the optical contrast at 780 nm by a significant margin. In contrast, nearly all the dopants led to a lower contrast at the two shorter wavelengths. The exception to this was V, which slightly improved the optical contrast at 650 nm. This general reduction in contrast could result from two different effects. TM atoms with partially-filled d orbitals—including the majority of the dopants, according to the results in figure 1—may absorb at either of these wavelengths, particularly 405 nm, through d–d electronic transitions, or through transitions between the host valence band and low-lying d states in the conduction band.

Alternatively, the reduction in contrast could also come about through the influence of the TM atoms on the structure of the host. This latter point may be understood within a model developed by Shportko *et al* [52], whereby the contrast in PCMs is ascribed to a large electronic polarizability in the crystalline phase, arising from electron-deficient (‘resonant’)

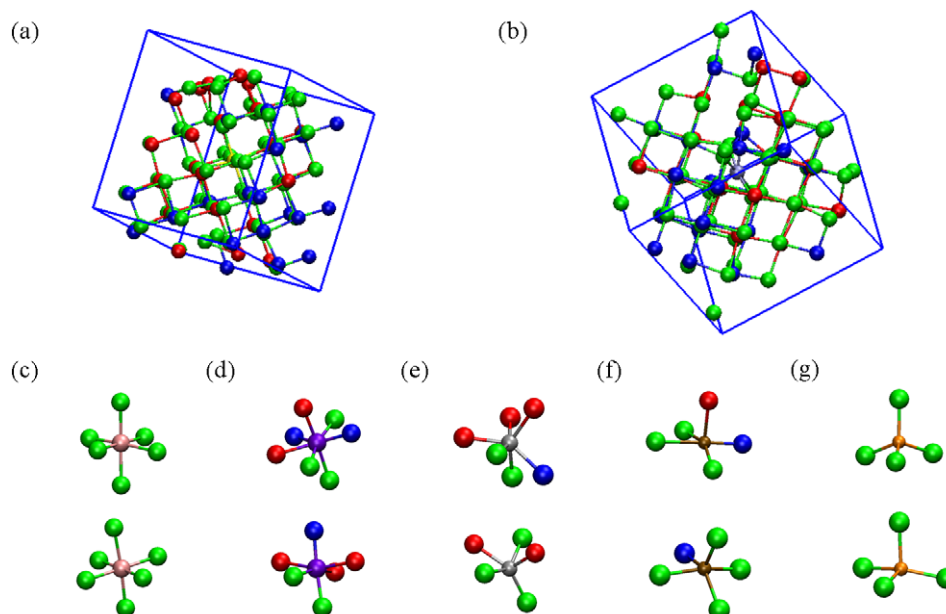


Figure 4. Structure and bonding in transition-metal (TM)-doped $\text{Ge}_2\text{Sb}_2\text{Te}_5$. The upper images show snapshots of relaxed crystalline models of (a) Sc- and (b) V-doped $\text{Ge}_2\text{Sb}_2\text{Te}_5$. The lower images show close-ups of the local atomic geometries around (c) Cr, (d) Co, (e) Ni, (f) Cu and (g) Zn in relaxed amorphous (top) and crystalline (bottom) models. The snapshots were taken using the VMD software [54]. The colour coding of the host atoms is as follows: Ge—blue, Sb—red, Te—green. The TM atoms are coloured as in figure 1.

p-bonding. If the TM dopants are unable to integrate fully into the crystalline structure, and thus introduce significant structural distortions, this would reduce the extent of the resonant bonding, and hence decrease the reflectance of the crystalline phase compared to that of the amorphous one. In keeping with this, a comparison of the reflectance spectra of the ten doped systems indicates that the TM atoms lead to larger variations in the crystalline-phase reflectance than in the amorphous-phase one (see footnote 1). We note that, if the reduction in contrast arises predominantly through structural modification of the crystalline phase, it is possible that our models may be too small to model accurately the effect of the TM atoms on reflectance as, in a larger system, it would be possible for the dopants to segregate to the edges of crystalline regions, and thus have a less pronounced effect on its structure. This could be clarified by running simulations on larger models.

These results suggest that many first-row TM dopants might not yield a useful improvement in the optical properties of $\text{Ge}_2\text{Sb}_2\text{Te}_5$ at the 650 and 405 nm wavelengths currently in use. However, if the microscopic explanation discussed here is correct, it establishes a general principle for selecting dopants which would enhance these properties—suitable dopants should not possess electronic configurations which might lead to absorption in the visible spectrum, and should also either integrate completely into the crystalline host material, or reside at the periphery of the structure, thereby having a minimal impact on structural order.

5. Structure and bonding

The TMs adopt a range of geometries in their minerals, e.g. octahedral and tetrahedral environments [53], and it is

therefore interesting to investigate the complexes formed by the ten TM dopants in a $\text{Ge}_2\text{Sb}_2\text{Te}_5$ host. Figure 4 presents a range of illustrative snapshots from our relaxed amorphous and crystalline models.

All the simulated doped systems crystallized within 500 ps, indicating that all ten TMs do not inhibit the crystallization of the host material, at least at low concentrations (see footnote 1). Our simulated annealing invariably yielded the metastable cubic crystal structure, rather than the high-temperature equilibrium hexagonal form. The former is thought to be the crystal structure formed in PCM devices, primarily due to rapid heating rates during crystallization [8]. Indeed, the rocksalt structure has been similarly observed in other AIMD annealing simulations (e.g. [33, 34, 39]). Although it is possible that a cubic simulation cell, as is typically employed in AIMD simulations of $\text{Ge}_2\text{Sb}_2\text{Te}_5$, might favour one structure over another, the orientation of the crystals formed during our simulations was variable, and the crystal axes were generally not parallel to the cell sides (see footnote 1). This suggests that, as noted in [34], the simulation cell shape may not exert a large influence during the crystallization. We also observed no conversion to the hexagonal structure when the crystalline models were energy-relaxed.

In the amorphous phase, the dopant atoms are likely to be able to adopt their preferred local geometries, while in the crystalline phase, their ability to do so may be constrained by the long-range order. In principle, the metastable cubic rocksalt structure of crystalline GST provides six-coordinate (octahedral) substitutional/vacancy sites and eight-coordinate interstices. Vacant octahedral sites are a natural location for cationic dopant atoms to reside, since there are intrinsically 20% vacancies on the cationic sublattice. However, these

vacancies could potentially cluster, providing larger voids in which dopant atoms, including those with a low positive, or even negative, charge, could adopt a more flexible range of geometries. We observed all three of these possibilities in our crystalline models, suggesting that crystalline $\text{Ge}_2\text{Sb}_2\text{Te}_5$ is in fact quite flexible at accommodating TM dopants.

We found that elements Sc to Co adopted distorted octahedral geometries in the amorphous phase, while Ni and Cu formed complexes with an approximately square-based pyramidal geometry, and Zn formed tetrahedral complexes. The amorphous-phase geometries were largely maintained in the crystalline models, with the atoms occupying a mix of the possible sites (see footnote 1). Sc integrated completely into the structure, occupying cationic sites, while Mn adopted distorted octahedral sites, but adjacent to voids. V and Fe took up interstitial sites, although again these were heavily distorted, and located at the periphery of the crystal. We found that Ti, Cr and Co adopted both interstitial and octahedral sites in our simulations, in both cases invariably located adjacent to voids. Ni, Cu and Zn displayed much less of an affinity for crystal-structure sites, instead being accommodated within large voids and forming complexes with the atoms at the edge of the defects and suggesting that, in a bulk system, these atoms may locate near grain boundaries. Larger models than those used here would be needed to confirm this, however.

We note that, for Cr, Fe, Co and Ni, the crystalline geometries observed in our simulations are, at least in part, at odds with the results of the studies performed in [38, 40], in which dopant atoms were placed into ideal models of cubic $\text{Ge}_2\text{Sb}_2\text{Te}_5$ ‘by hand’. This difference may indicate a significant kinetic barrier to incorporating these ions completely into the crystal structure, or it could be due to the density being lower than the optimum crystalline one during the annealing. However, our simulated annealing procedure allows the dopant atoms more structural flexibility, in particular the possibility of residing near vacancies or voids, which could also account for the discrepancy.

To investigate this further, we conducted a simple site-preference study (see footnote 1). We took a model of undoped crystalline $\text{Ge}_2\text{Sb}_2\text{Te}_5$, generated by the AIMD annealing procedure used for the doped systems, and generated models in which the TM atoms were substituted for octahedral Ge, Sb and Te atoms, or placed in interstitial and vacancy sites. Their total energies were then compared after relaxation. This study is similar to those reported in [38, 40], although the crystalline model from the AIMD annealing simulation was not ideal, containing distortions and large clusters of vacancies.

Of the three possible substitution sites, elements Sc to Fe exhibited significant energetic preferences, on the order of 10–20 meV per atom, for cationic sites. The preference was rather less marked for the later TMs, which could be due to some of these atoms preferring to complex with Ge/Sb and/or to adopt non-octahedral geometries. Surprisingly, on comparing the interstitial and vacancy sites, we found that elements Sc to Co appeared to prefer the former. The vacant site in our model had an imperfect octahedral coordination, and thus was non-ideal in that sense, which could explain this

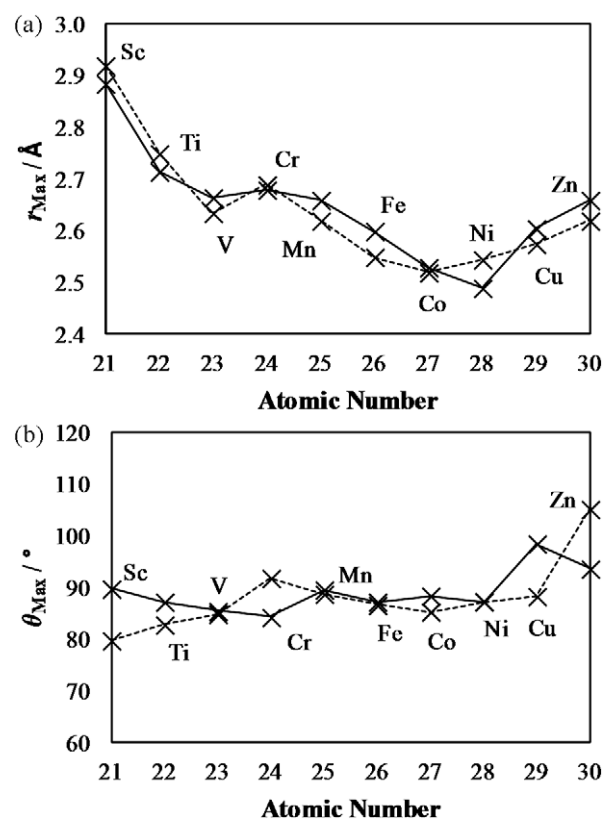


Figure 5. Structural properties of transition-metal (TM)-doped $\text{Ge}_2\text{Sb}_2\text{Te}_5$. (a) Position of the first maxima in the TM partial radial distribution function curves for amorphous (dashed line) and crystalline (solid line) models, as a function of atomic number. (b) Position of the maximum in the TM bond-angle distribution curves for the two phases; the shading of the lines is as in (a). The distributions in (b) were computed using a 3.5 Å cut-off radius to define the first coordination sphere. All analyses were averaged over 4000 frames, corresponding to 20 ps of MD data, and the values are the average of those obtained from both sets of simulation data (see footnote 1).

finding in part, but it may also reinforce the point made above about there being a kinetic barrier to occupying interstitial sites. For many of the atoms, the preference for one site over another was quite small, and thus in a bulk system, a fraction of the dopant atoms may well be found in both sites. This was evident in our simulations, in which some TMs were observed in both cationic and interstitial sites.

To study structural properties more systematically, we computed partial radial distribution functions (RDFs) and bond-angle distributions (BADs) for each TM atom in both phases. The positions of the first maxima in the partial RDFs are indicative of the average TM bond lengths, while the positions of the main peaks in the BADs reflect preferential coordination geometries. These quantities are plotted, as a function of atomic number, in figure 5.

There is a general reduction in bond lengths from elements Sc to Co, which can be ascribed to an increase in nuclear charge, and corresponding decrease in TM atomic radius, as the period is traversed. There is a sharp drop in bond length between Sc and Ti, which explains why Sc (with a Sc–Te bond length close to the estimated average bond length

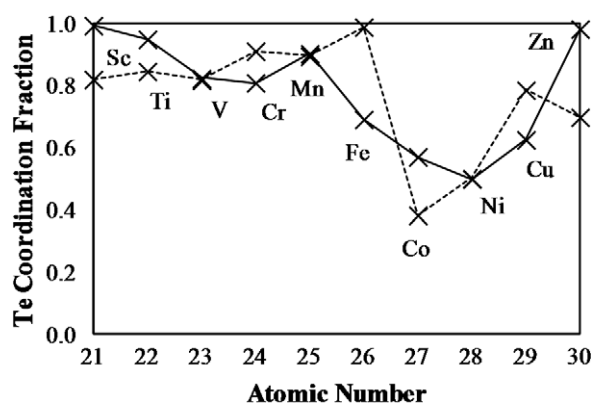


Figure 6. Fractions of the transition-metal (TM) coordination shells made up by Te atoms in amorphous (dashed line) and crystalline (solid line) models of TM-doped $\text{Ge}_2\text{Sb}_2\text{Te}_5$, as a function of atomic number. These analyses were averaged over 20 ps of MD data, and the plot shows the average of the fractions obtained from both sets of simulations (see footnote 1).

in undoped crystalline $\text{Ge}_2\text{Sb}_2\text{Te}_5$ (see footnote 1)) integrates into the crystal structure, but the other octahedral dopants tend to reside near voids; at the periphery of the structure, their preferred shorter bond lengths could be accommodated with minimal distortion. The elements Ni to Zn do not follow the decreasing trend, which is likely due to the different geometries that these elements adopt. Interestingly, there is generally little change in bond length on crystallization, suggesting that the structure of the host material does not exert a large influence on this.

The BAD curves indicate that some of the octahedral complexes formed by elements Sc to Co exhibit significant distortions, deviating by as much as 10° from the ideal octahedral 90° bond angle. For the later elements, an increasing trend is seen in the amorphous-phase bond angles, indicating a switch to geometries with smaller coordination numbers.

The variation in bond angles for the octahedral elements in the crystalline phase is smaller, suggesting that, in contrast to the bond lengths, the crystal structure does significantly influence dopant geometry.

Finally, figure 4 suggests that some TMs form complexes including a significant fraction of Ge/Sb atoms, which is unusual, given that Te is the (most) anionic species. To quantify this, we used the numerical integrals of partial RDFs to estimate the fraction of Te atoms in the first coordination spheres (figure 6), the radii of which were taken as the first minima in the TM partial RDFs. This analysis shows that the majority of the TMs bond preferentially to Te, with this element making up at least 80% of the coordination sphere, but that Co and Ni are notable exceptions, being coordinated by a high proportion of Ge and Sb atoms. Fe and Cu exhibit more marginal affinities for these atoms, although for the former, this may be due to its propensity for occupying interstices.

These coordination preferences are also reflected in the calculated Bader atomic charges [55] of the TM atoms (figure 7), with Co and Ni having a slight negative charge.

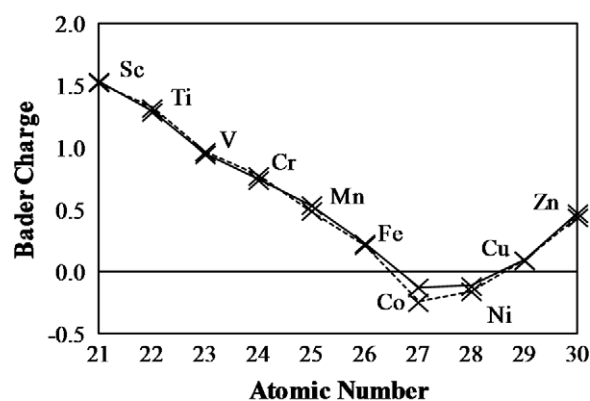


Figure 7. Calculated Bader atomic charges [55] of the dopant atoms in relaxed models of amorphous (dashed line) and crystalline (solid line) transition metal-doped $\text{Ge}_2\text{Sb}_2\text{Te}_5$, as a function of atomic number. The charges are the average of the values obtained from both sets of simulations (see footnote 1).

For elements Sc to Co, which prefer octahedral geometries, there is an almost linear decrease in the TM charge with atomic number, which can be naturally explained by their increasing nuclear charge. The charge increases again for elements from Ni–Zn, which can be ascribed to their reduced coordination number, plus the fact that Cu and Zn notionally have a complete d shell which would make them less readily able to attain high oxidation states.

6. Dynamics

In previous work [39], it was noted that Zn could exhibit significant atomic motion after crystallization of the host matrix had completed. In the present simulations, we observed similar behaviour for several other TM dopants (see footnote 1), with the TM atomic mean-square displacements (MSDs) exhibiting significant fluctuations after crystallization. The displacements were most pronounced for Ni and Cu, as well as Zn, suggesting, as noted in [39], that the atomic motion may be exacerbated by a preference for non-octahedral geometry. However, since we found that many of the TM dopants preferring octahedral coordination were located near to voids, even when integrated into the crystal, it is not unreasonable to expect that this behaviour might be observed for these elements as well.

Figure 8 shows the MSD curve for the Ni atom during annealing of the Ni-doped system. From the structural models, it can be seen that the motion is due to Ni ‘hopping’ between sites within the host lattice. The atom adopts a number of positions, forming complexes in which it appears to be integrated substitutionally into the crystal structure, and complexes where it takes up a more ‘interstitial-like’ coordination.

This shows that, for at least some of the first-row TMs, the geometry within the crystal structure is not fixed, and the dopant atoms may move within the structure, hopping between different sites. The motion is quite likely to be assisted by the presence of adjacent voids, which would facilitate the requisite atomic rearrangements. This TM

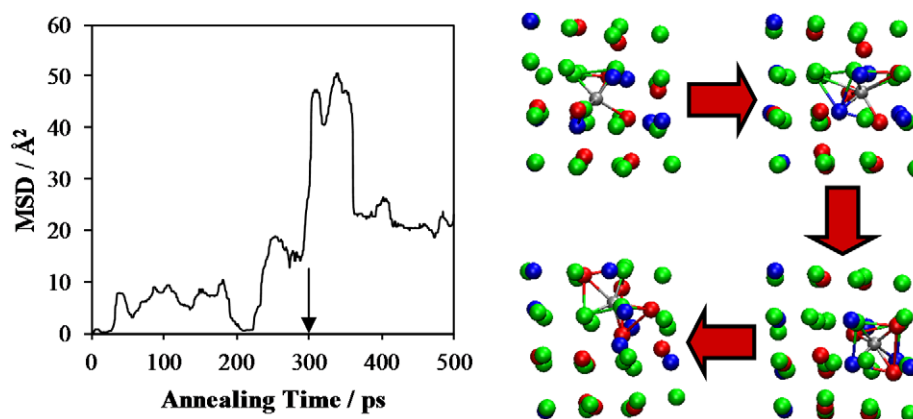


Figure 8. Atomic dynamics in crystalline Ni-doped $\text{Ge}_2\text{Sb}_2\text{Te}_5$. Even after crystallization, the Ni atom displays significant atomic motion, as evident from the Ni mean-square displacements (left). In this graph, the vertical arrow on the time axis denotes the point at which the crystallization of the host system completed. The motion occurs by the dopant atom ‘hopping’ between different complexes at various positions within the host lattice (right). The colour coding of the atoms is as in figure 4, and the structural snapshots were prepared using the VMD software [54].

motion may be of interest for device applications, since it could introduce low-frequency ‘rattling’ phonon modes, as seen in systems such as CoSb_3 [56], which could decrease the thermal conductivity and thereby help to improve thermal confinement and reduce thermal ‘cross-talk’ between adjacent cells.

7. Summary

The results of this work illustrate how the systematic study of an entire family of related dopants can help to identify trends and patterns in both their microscopic behaviour within the host, and their influence on its physical properties. For the first-row transition metals, the trends are invariably related to the increase in nuclear charge, and the corresponding decrease in atomic radius, on moving from Sc to Zn.

As the period is traversed, the TM d states change in energy, such that they go from being located almost entirely within the host conduction band for Sc, to being deep within the valence band for Zn. Although their contribution to the overall form of the host DOS is small, due to their low atomic concentration, since many of the TMs atoms contribute states near the Fermi level, they might be used subtly to alter the form of the band tails and correspondingly influence those properties which depend on the bandgap, such as electrical conductivity and optical reflectance. We found that elements from V to Fe could have magnetic ground-states in both amorphous and crystalline phases, potentially giving an additional property contrast between them, and thereby allowing PCRAM to become part of spintronic devices.

According to our simulations, while most of the TM dopants yield an increase in optical contrast at the compact disc wavelength of 780 nm, they generally reduce the contrast at the other technologically-relevant wavelengths of 650 and 405 nm. Based on our findings, we suggest that, to enhance the optical contrast in $\text{Ge}_2\text{Sb}_2\text{Te}_5$, dopants with electronic configurations that lend themselves to absorbing in the visible spectrum should be avoided, and effective dopants

might be those which do not disturb the structural order in the crystalline phase, thereby ensuring a high degree of electronic delocalization. Suitable dopants could be those which integrate into the structure with a minimal degree of distortion, or which preferentially reside at the periphery of the crystal.

The decrease in atomic radius on moving across the period naturally leads to a decrease in the TM-centred bond length, and the smaller atomic radii of Co, Ni, Cu and Zn leads to a progressive change in geometry from sixfold-coordinated octahedral coordination for Co to a fourfold-coordinated tetrahedral coordination for Zn. The increasing nuclear charge also leads to an increased electronegativity, reflected in a decrease in the TM charges on going from Sc to Co. The elements Co and Ni are unique in having slightly negative charges and, unusually, exhibit a preference for coordinating to Ge/Sb, as well as Te. These trends reverse for Ni, which can be explained by a tendency for Cu and Zn to prefer a filled d shell.

Our simulation results suggest that crystalline $\text{Ge}_2\text{Sb}_2\text{Te}_5$ is somewhat flexible in accommodating TM dopant atoms, and we observed TMs occupying both vacancy and interstitial sites. A general observation in our results is that TM atoms, whose bond lengths or geometrical preferences do not fit with the metastable cubic rocksalt structure of GST, tend to be located near to voids, allowing them to be accommodated with minimal structural distortion. In a bulk system, it is possible that dopants whose preferred bonding geometries are a poor match for the host crystalline material might segregate to grain boundaries, integrating into the periphery of the crystal structure.

Finally, we observed that, as reported in previous work [39], some of the atoms which do not integrate well into the crystalline structure display pronounced atomic thermal motion after crystallization of the host has completed, dynamically adopting a range of coordination geometries. This bears a resemblance to the unusual lattice dynamics of compounds with caged ions, where the

consequent low-frequency ‘rattling’ phonons give rise to a low thermal conductivity. This potential enhancement of thermal confinement could be valuable in reducing thermal ‘cross-talk’ between memory cells in devices.

The comprehensive elemental simulational survey presented here has shown that TM doping could lead to a number of useful property enhancements in $\text{Ge}_2\text{Sb}_2\text{Te}_5$ phase-change materials. The fact that TMs represent a large family of similar dopants, in conjunction with the trends and patterns identified in this study, opens up the possibility of selecting a dopant, or combination of dopants, to optimize material properties for specific applications. The computational approach used here is general, and could be used in the future to investigate other families of dopants for materials-design purposes.

Acknowledgments

The authors gratefully acknowledge helpful discussions with D Loke and Dr T H Lee. JMS is indebted to Trinity College, Cambridge for the provision of an Internal Graduate Studentship. This work was performed using the University of Cambridge High Performance Computing Service (www.hpc.cam.ac.uk), and was funded in part from grants provided by the UK Engineering and Physical Sciences Research Council.

References

- [1] Lacaíta A L and Wouters D J 2008 Phase-change memories *Phys. Status Solidi a* **205** 2281–97
- [2] Ovshinsky S R 1968 Reversible electrical switching phenomena in disordered structures *Phys. Rev. Lett.* **21** 1450–3
- [3] Wang W J, Shi L P, Zhao R, Lim K G, Lee H K, Chong T C and Wu Y H 2008 Fast phase transitions induced by picosecond electrical pulses on phase change memory cells *Appl. Phys. Lett.* **93** 043121
- [4] Loke D, Lee T H, Wang W J, Shi L P, Zhao R, Yeo Y C, Chong T C and Elliott S R 2012 Breaking the speed limits of phase-change memory *Science* **336** 1566–9
- [5] Feng X, Liao A D and Estrada D 2011 Low-power switching of phase-change materials with carbon nanotube electrodes *Science* **331** 568–70
- [6] Chong T C, Shi L P, Zhao R, Tan P K, Li J M, Lee H K, Miao X S, Du A Y and Tung C H 2006 Phase change random access memory cell with superlattice-like structure *Appl. Phys. Lett.* **88** 122114
- [7] Caldwell M A, Jeyasingh R G D, Wong H S P and Milliron D J 2012 Nanoscale phase change memory materials *Nanoscale* **4** 4382–92
- [8] Nirschl T, Philipp J B, Flapp T D, Burr G W, Rajendran B, Leao M H, Schrott A, Yang M, Breitwisch M, Chen C F, Joseph E, Lamorey M, Cheek R, Chen S H, Zaidi S, Raoux S, Chen Y C, Zhu Y, Bergmann R, Lung H L and Lam C 2007 Write strategies for 2 and 4-bit multi-level phase-change memory 2007 *IEEE Int. Electron Devices Mrg vol 1 and 2*, pp 461–4
- [9] Wuttig M 2005 Phase-change materials—towards a universal memory? *Nature Mater.* **4** 265–6
- [10] Wong H S P, Raoux S, Kim S, Liang J L, Reifengberg J P, Rajendran B, Asheghi M and Goodson K E 2010 Phase change memory *Proc. IEEE* **98** 2201–27
- [11] Yamada N, Ohno E, Nishiuchi K, Akahira N and Takao M 1991 Rapid-phase transitions of $\text{GeTe-Sb}_2\text{Te}_3$ pseudobinary amorphous thin-films for an optical disk memory *J. Appl. Phys.* **69** 2849–56
- [12] Iwasaki H, Ide Y, Harigaya M, Kageyama Y and Fujimura I 1992 Completely erasable phase-change optical disk *Japan. J. Appl. Phys.* **31** 461–5
- [13] Burr G W, Breitwisch M J, Franceschini M, Garetto D, Gopalakrishnan K, Jackson B, Kurdi B, Lam C, Lastras L A, Padilla A, Rajendran B, Raoux S and Shenoy R S 2010 Phase change memory technology *J. Vac. Sci. Technol. B* **28** 223–62
- [14] Papandreou N, Pozidis H, Mittelholzer T, Close G F, Breitwisch M, Lam C and Eleftheriou E 2011 2011 3rd *IEEE Int. Memory Workshop* (Piscataway, NJ: IEEE) p 4
- [15] Raoux S, Cheng H Y, Caldwell M A and Wong H S P 2009 Crystallization times of Ge–Te phase change materials as a function of composition *Appl. Phys. Lett.* **95** 071910
- [16] Cheng H-Y, Raoux S and Jordan-Sweet J L 2011 The crystallization behavior of stoichiometric and off-stoichiometric Ga–Sb–Te materials for phase-change memory *Appl. Phys. Lett.* **98** 121911
- [17] Suzuki E, Miura H, Harigaya M, Ito K, Iwata N and Watada A 2005 In–Sb phase-change material for 16x rewritable digital versatile disk *Japan. J. Appl. Phys.* **44** 3598–600
- [18] Chang C C, Chang P C, Kao K F, Yew T R, Tsai M J and Chin T S 2011 C–Sb materials as candidate for phase-change memory *IEEE Trans. Magn.* **47** 645–8
- [19] Chang C C, Hung C Y, Kao K F, Tsai M J, Yew T R and Chin T S 2010 Phase transformation in Mg–Sb thin films *Thin Solid Films* **518** 7403–6
- [20] Borisenko K B, Chen Y X, Cockayne D J H, Song S A and Jeong H S 2011 Understanding atomic structures of amorphous C-doped $\text{Ge}_2\text{Sb}_2\text{Te}_5$ phase-change memory materials *Acta Mater.* **59** 4335–42
- [21] Liu B, Zhang T, Xia J L, Song Z T, Feng S L and Chen B 2004 Nitrogen-implanted $\text{Ge}_2\text{Sb}_2\text{Te}_5$ film used as multilevel storage media for phase change random access memory *Semicond. Sci. Technol.* **19** L61–4
- [22] Jeong T H, Seo H, Lee K L, Choi S M, Kim S J and Kim S Y 2001 Study of oxygen-doped GeSbTe film and its effect as an interface layer on the recording properties in the blue wavelength *Japan. J. Appl. Phys.* **40** 1609–12
- [23] Feng J, Zhang Y, Qiao B W, Lai Y F, Lin Y Y, Cai B C, Tang T A and Chen B 2007 Si doping in $\text{Ge}_2\text{Sb}_2\text{Te}_5$ film to reduce the writing current of phase change memory *Appl. Phys. A* **87** 57–62
- [24] Shingai H, Kato T, Kosuda M, Takagi Y, Oyake H and Hirata H 2010 Triple-layer rewritable disc with Sb-based phase-change material *Japan. J. Appl. Phys.* **49** 08KG02
- [25] Song W D, Shi L P, Miao X S and Chong C T 2008 Synthesis and characteristics of a phase-change magnetic material *Adv. Mater.* **20** 2394–7
- [26] Men L, Tominaga J, Fuji H, Kikukawa T and Atoda N 2001 The effects of metal-doped GeSbTe films on light scattering-mode super-resolution near-field structure (super-RENS) *Japan. J. Appl. Phys.* **40** 1629–33
- [27] Huang Y-J, Chen Y-C and Hsieh T-E 2009 Phase transition behaviors of Mo- and nitrogen-doped $\text{Ge}_2\text{Sb}_2\text{Te}_5$ thin films investigated by *in situ* electrical measurements *J. Appl. Phys.* **106** 034916
- [28] Chappert C, Fert A and Van Dau F N 2007 The emergence of spin electronics in data storage *Nature Mater.* **6** 813–23
- [29] Akola J, Jones R O, Kohara S, Kimura S, Kobayashi K, Takata M, Matsunaga T, Kojima R and Yamada N 2009 Experimentally constrained density-functional calculations of the amorphous structure of the prototypical phase-change material $\text{Ge}_2\text{Sb}_2\text{Te}_5$ *Phys. Rev. B* **80** 020201
- [30] Matsunaga T, Akola J, Kohara S, Honma T, Kobayashi K, Ikenaga E, Jones R O, Yamada N, Takata M and Kojima R 2011 From local structure to nanosecond recrystallization

- dynamics in AgInSbTe phase-change materials *Nature Mater.* **10** 129–34
- [31] Krbal M, Kolobov A V, Fons P, Tominaga J, Elliott S R, Hegedus J and Uruga T 2011 Intrinsic complexity of the melt-quenched amorphous $\text{Ge}_2\text{Sb}_2\text{Te}_5$ memory alloy *Phys. Rev. B* **83** 054203
- [32] Akola J and Jones R O 2007 Structural phase transitions on the nanoscale: the crucial pattern in the phase-change materials $\text{Ge}_2\text{Sb}_2\text{Te}_5$ and GeTe *Phys. Rev. B* **76** 235201
- [33] Lee T H and Elliott S R 2011 *Ab initio* computer simulation of the early stages of crystallization: application to $\text{Ge}_2\text{Sb}_2\text{Te}_5$ phase-change materials *Phys. Rev. Lett.* **107** 145702
- [34] Hegedus J and Elliott S R 2008 Microscopic origin of the fast crystallization ability of Ge–Sb–Te phase-change memory materials *Nature Mater.* **7** 399–405
- [35] Lee T H and Elliott S R 2011 Structural role of vacancies in the phase transition of $\text{Ge}_2\text{Sb}_2\text{Te}_5$ memory materials *Phys. Rev. B* **84** 094124
- [36] Cho E, Han S, Kim D, Horii H and Nam H S 2011 *Ab initio* study on influence of dopants on crystalline and amorphous $\text{Ge}_2\text{Sb}_2\text{Te}_5$ *J. Appl. Phys.* **109** 043705
- [37] Eunae C, Yong Y and Seungwu H 2011 Enhanced amorphous stability of carbon-doped $\text{Ge}_2\text{Sb}_2\text{Te}_5$: *ab initio* investigation *Appl. Phys. Lett.* **99** 183501
- [38] Li Y and Mazzarello R 2012 Magnetic contrast in phase-change materials doped with Fe impurities *Adv. Mater.* **24** 1429–33
- [39] Skelton J M, Lee T H and Elliott S R 2012 Structural, dynamical, and electronic properties of transition metal-doped $\text{Ge}_2\text{Sb}_2\text{Te}_5$ phase-change materials simulated by *ab initio* molecular dynamics *Appl. Phys. Lett.* **101** 024106
- [40] Zhang W, Ronneberger I, Li Y and Mazzarello R 2012 Magnetic properties of crystalline and amorphous phase-change materials doped with 3D impurities *Adv. Mater.* **24** 4387–91
- [41] Kresse G and Hafner J 1993 *Ab initio* molecular-dynamics for liquid–metals *Phys. Rev. B* **47** 558–61
- [42] Perdew J P, Burke K and Ernzerhof M 1996 Generalized gradient approximation made simple *Phys. Rev. Lett.* **77** 3865–8
- [43] Blochl P E 1994 Projector augmented-wave method *Phys. Rev. B* **50** 17953–79
- [44] Monkhorst H J and Pack J D 1976 Special points for Brillouin-zone integrations *Phys. Rev. B* **13** 5188–92
- [45] Kohn W and Sham L J 1965 Self-consistent equations including exchange and correlation effects *Phys. Rev.* **140** 1133–8
- [46] Seidl A, Gorling A, Vogl P, Majewski J A and Levy M 1996 Generalized Kohn–Sham schemes and the band-gap problem *Phys. Rev. B* **53** 3764–74
- [47] Ding D, Bai K, Song W D, Shi L P, Zhao R, Ji R, Sullivan M and Wu P 2011 Origin of ferromagnetism and the design principle in phase-change magnetic materials *Phys. Rev. B* **84** 214416
- [48] Fukuma Y, Asada H, Arifuku M and Koyanagi T 2002 Carrier-enhanced ferromagnetism in $\text{Ge}_{1-x}\text{Mn}_x\text{Te}$ *Appl. Phys. Lett.* **80** 1013–5
- [49] Chen W Q, Teo K L, Jalil M B A and Liew T 2006 Compositional dependencies of ferromagnetic $\text{Ge}_{1-x}\text{Mn}_x\text{Te}$ grown by solid-source molecular-beam epitaxy *J. Appl. Phys.* **99** 08D515
- [50] Tong F, Hao J H, Chen Z P, Gao G Y and Miao X S 2011 Phase-change control of ferromagnetism in GeTe-based phase change magnetic thin-films by pulsed laser deposition *Appl. Phys. Lett.* **99** 081908
- [51] Wang K, Wamwangi D, Ziegler S, Steimer C and Wuttig M 2004 Influence of Bi doping upon the phase change characteristics of $\text{Ge}_2\text{Sb}_2\text{Te}_5$ *J. Appl. Phys.* **96** 5557–62
- [52] Shportko K, Kremers S, Woda M, Lencer D, Robertson J and Wuttig M 2008 Resonant bonding in crystalline phase-change materials *Nature Mater.* **7** 653–8
- [53] Szwacki N G, Przedziecka E, Dynowska E, Boguslawski P and Kossut J 2004 Structural properties of MnTe, ZnTe, and ZnMnTe *Acta Phys. Pol. A* **106** 233–8
- [54] Humphrey W, Dalke A and Schulten K 1996 VMD: visual molecular dynamics *J. Mol. Graph.* **14** 33–8
- [55] Bader R F 1990 *Atoms in Molecules: A Quantum Theory* (Oxford: Oxford University Press)
- [56] Lu P X, Ma Q H, Li Y A and Hu X 2010 A study of electronic structure and lattice dynamics of CoSb_3 skutterudite *J. Magn. Magn. Mater.* **322** 3080–3